2002

Comparison of Na Lidar and Meteor Radar Wind Measurements at Starfire Optical Range, NM, USA

Alan Z. Liu
Embry Riddle Aeronautical University - Daytona Beach, liuz2@erau.edu

Wayne K. Hocking

Steven J. Franke

T. Thayaparan

PERGAMON

Journal of Atmospheric and Solar-Terrestrial Physics 64 (2002) 31–40

Journal of ATMOSPHERIC AND SOLAR-TERRESTRIAL PHYSICS

www.elsevier.com/locate/jastp

Comparison of Na lidar and meteor radar wind measurements at Starfire Optical Range, NM, USA

Alan Z. Liu[a,*], Wayne K. Hocking[b], Steven J. Franke[a], T. Thayaparan[c]

[a] *Department of Electrical and Computer Engineering, University of Illinois at Urbana-Champaign, Urbana, IL, USA*
[b] *University of Western Ontario, Canada*
[c] *Defense Research Establishment, Ottawa, Canada*

Received 20 February 2001; received in revised form 26 September 2001; accepted 18 October 2001

Abstract

Simultaneous wind measurements in the mesopause region at Starfire Optical Range near Albuquerque, NM with Na wind/temperature lidar and meteor radar have been performed and compared. 20 nights of hourly data recorded with these two instruments at two layers around 86 and 93 km altitude are compared for both zonal and meridional wind components. The mean values are found to have no statistically significant differences. The correlation coefficients vary between 0.63 and 0.70, indicating that the two sets of measurements are broadly consistent. When comparing the averaged variations over the night, the two measurements are highly correlated, with correlation coefficients varying from 0.84 to 0.95. It indicates that the strong tidal variation is well captured by both instruments. Differences are however significant at individual hours, which are believed to be mainly due to the fact that the meteor radar wind is an average over the entire sky while the lidar measures wind within a volume about 100 m in diameter.

Keywords: Meteor radar; Na lidar; Mesopause wind; Linear regression; Tidal variation

1. Introduction

Several techniques exist for the measurement of middle atmosphere winds from ground based stations, including (among others) meteor radar (e.g. Roper, 1975; Cervera and Reid, 1995; Hocking and Thayaparan, 1997; Hocking et al., 2001a), MF radar (e.g. Briggs, 1984; Hocking et al., 1989; Phillips et al., 1994; Holdsworth, 1999) and lidar (e.g. Gardner et al., 1989; Bills et al., 1991a; She and Yu, 1994; Gardner and Papen, 1995). Depending on instrumentation, these techniques produce spatial averages over different volumes of the atmosphere, and all have advantages and disadvantages. Comparisons among these different techniques are very useful for understanding and making better use of the respective measurements. Wind-measuring instruments are situated at many sites, covering a wide geographical range, but it is rather rare for such instruments to be co-located, and in general measurements made by these instruments do not overlap spatially. Between June 1998 and November 2000, measurements have been made by meteor radar and Na lidar at Starfire Optical Range (SOR), which is located on the Kirtland Air Force Base (35°N, 106.5°W), near Albuquerque, NM. These simultaneous measurements provide a good opportunity for comparison between the two measurement techniques, which can in turn provide guidance for the interpretation and application of these two wind measurement methods in more general situations.

We report here wind comparisons that cover 20 nights of temporally simultaneous data, beginning in September 1998. The measurement techniques are described in the following section. Section 3 describes our comparison methods and the theory used for our regression analysis. Our results are presented in Section 4, followed by conclusions.

* Corresponding author. Tel.: +1-217-333-6982; fax: +1-217-333-4303.
E-mail address: liuzr@uiuc.edu (A.Z. Liu).

1364-6826/02/$ - see front matter
PII: S1364-6826(01)00095-5

2. Measurement techniques and data preparation

2.1. Meteor radar winds

The meteor radar used for our wind determinations was a commercially produced SKiYMET radar, designed for all-sky real-time meteor detection. It is currently owned and operated by Mardoc Inc., and leased to the University of Western Ontario. The system is described in considerable detail by Hocking et al. (2001a). In brief, the system employs a 6 kW peak-power transmitter at 35.24 MHz, which transmits radio pulses with a length of 13 μs (giving a resolution of 2 km) through a single, vertically directed three-element Yagi antenna with a broad polar diagram, and receives backscattered signal on five separated two-element Yagis. The five receiving antennas are arranged in the form of an asymmetric cross, with two perpendicular arms having lengths of 2.0 wavelengths, and the other pair of perpendicular arms having lengths of 2.5 wavelengths (see Hocking et al., 2001a). The cross is aligned at 2° clockwise from a north–south–east–west alignment. Each receiving antenna is connected to a separate radio receiver with a cable of length 70 m, where each cable has been cut to have equal phase-lengths. Signals received on each antenna can therefore be compared and used in interferometric applications. Whenever a meteor trail appears in the sky with a suitable alignment, the transmitted pulses of radiation are reflected back to the ground, where separate signals are digitized from each receiver as in-phase and quadrature components. By comparing the amplitudes and phases recorded by each receiver, it is possible to use interferometry to determine the location of the meteor in the sky.

The pulse repetition frequency (PRF) used is 2143 Hz, which is unusually high for meteor radars. This high PRF gives us a considerable improvement in meteor delectability, but also produces an aliasing range of 70 km. Thus it should be impossible to resolve whether a meteor had a range of say 65, 135, 205 km, etc. This limitation, however, is easily resolved. Because it is known that at VHF most meteors are observed in the altitude range between 70 and 110 km, and because the angular location (azimuth and elevation) are well known from interferometry, it is possible in most cases to use this information to determine the true range unambiguously.

The whole system is controlled by a UNIX operating system running on a personal computer. The system software has been carefully designed for meteor detection, and can discriminate true meteor echoes from other impulsive phenomena like interference and lightning with better than 99% accuracy. The system can even function efficiently in severe lightning storms.

Once the meteors have been identified, a variety of characteristics of the signals are parameterized, including the radial drift speed, the decay time, the amplitude, and (on occasion) the speed at which the meteor entered the atmosphere. By comparing the phases of the received signals on all five receivers, it is possible to use the principles of interferometry to determine the location of the meteor in the sky to an accuracy of better than ± 1.5–2° (e.g. see Jones et al., 1998). From these parameters, a second class of parameters may be derived, including upper atmosphere wind speeds, temperatures in the meteor region, and ambipolar diffusion coefficients.

Radial velocities are determined for subsequent horizontal wind calculations. Auto-correlations on single antennas, and cross-correlation functions between all possible pairs of antennas, are found for each meteor detection, and the rate of change of phase near zero lag is used to determine the radial velocity. The average of all of these estimates is then taken. The standard deviation for the mean is also found. This latter parameter is used as an estimate for the error, and is also stored along with the radial velocity for subsequent analysis. If, however, the standard deviation for the mean is excessively large (typically $> 5.5\ \mathrm{ms}^{-1}$) then the "meteor" is rejected entirely (see Hocking et al., 2001a).

Middle atmosphere winds are determined by collectively utilizing the radial velocities of meteors detected within a specified altitude-time window, and then combining them in an all-sky manner to determine upper level winds. For our comparisons here-in, we use a window of 1 hour and about 6 km. This low vertical resolution was necessary to compensate for the fact that SOR is a very noisy radio site.

The on-line all-sky least-squares fitting routine assumes a uniform wind field $\mathbf{u} = (u, v, w)$ and then minimizes the quantity

$$\sum_i (\mathbf{u} \cdot \mathbf{r}_i - v_i)^2, \tag{1}$$

where $\mathbf{r}_i$ is a unit vector pointing from the radar to the ith meteor trail, and v_i is the measured radial velocity. After the initial $\mathbf{u}$ is obtained, it is used to calculate $v_{\mathrm{m}i}$, the radial velocity the ith meteor should have if the mean wind was indeed $\mathbf{u}$. $v_{\mathrm{m}i}$ is then compared with v_i. If $|v_{\mathrm{m}i} - v_i| > 30\ \mathrm{ms}^{-1}$ then this meteor velocity is rejected as an outlier. Eq. (1) is then repeated, but only using meteors which pass the above test.

It is also useful to store the value of $\{\sum_i (v_{\mathrm{m}i} - v_i)^2/N\}^{1/2}$, where N is the total number of points. This parameter is called the "residual", and gives a measure of fluctuations of the wind speeds about the mean. It serves as a crude indicator of gravity wave and turbulence strengths.

2.2. Lidar winds

The horizontal winds were also measured with the University of Illinois Na wind/temperature lidar. The principle and techniques of measuring temperature and wind with the narrow band Na lidar are described in, e.g., Bills et al. (1991b) and Papen et al. (1995). In brief, the outgoing laser beam of the lidar transmitter tuned onto the Na D2 absorption line at about 589 nm can excite the resonant fluorescence from the neutral Na atoms distributed in the mesopause region (about

80–105 km altitude). The laser is periodically tuned to the peak frequency f_a of the Na D2 line and two wing frequencies $f_a \pm \Delta f$, where $\Delta f = 630$ MHz is about half of the full width at half maximum (FWHM) of the Na D2 Doppler broadened line. The returned photons from these three frequencies are collected and recorded by a receiver containing a telescope and a photon counting PMT. While all three signals are roughly proportional to the Na density, the ratios among these three signals can be used to determine the Na D2 line position and shape, which are related to the radial wind velocity (Doppler shift) and temperature (thermal broadening). Therefore Na density, temperature and radial wind velocity can be derived from the ratios of these three signals. The timing of returning signals gives the range information.

The Na lidar is coupled to the 3.5 m astronomical telescope at SOR so that the beam can be pointed in any direction following the telescope. The beam divergence is approximately 1 mrad, which gives a beam diameter (full width at e^{-2}) of 100 m at 100 km range. Typically the lidar is pointed to the zenith (Z), and at 10° off-zenith to the north (N), south (S), east (E) and west (W) in the sequence ZNEZSW. At each position, backscatter profiles are obtained with a 90 s integration time and 24 m range resolution. Approximately additional 30 s are required to point the telescope to the next position. This 6 position sequence is thus completed about every 12 min. The complete wind and temperature field can be derived every 6 min. To increase signal to noise ratio, the raw wind and temperature data are derived at a spatial resolution of 96 m. The temperature and wind are then binned to 500 m to further reduce the uncertainty due to photon noise.

Zonal (u) and meridional (v) components of the horizontal wind are calculated from radial winds measured at the off-zenith positions. The radial wind is related to the horizontal wind as follows:

$$V_E = u \sin\theta + w \cos\theta, \quad (2)$$

$$V_W = -u \sin\theta + w \cos\theta, \quad (3)$$

$$V_N = v \sin\theta + w \cos\theta, \quad (4)$$

$$V_S = -v \sin\theta + w \cos\theta, \quad (5)$$

where V_E, V_W, V_N and V_S are radial winds measured when the lidar beam was pointed to the east, west, north, and south off-zenith positions, respectively. w is the vertical wind measured when the lidar beam was pointed to the zenith. θ is the off-zenith angle associated with the off-zenith beams, which in our case is 10°.

Ideally, the horizontal wind components u and v should be calculated from Eqs. (2) to (5), which requires the zenith and off-zenith winds be obtained at the same time and same location. For the Na lidar however, it takes about 2 min to make a measurement in any one direction and then move to the next, and there is also about 15 km spatial difference between the zenith and off-zenith measurement points at 90 km altitude. Using radial winds and w at different time and location to calculate horizontal wind not only introduces error due to temporal and spatial variations of the wind file, but also increases the horizontal wind error by including the error from w measurement in addition to the radial wind measurement error. An alternative way, is to calculate the horizontal wind by simply assuming $w = 0$. The error of the calculated horizontal wind with this method includes the radial wind measurement error and the error that is related to the variance of w, but does not have the errors associated with temporal and spatial differences between radial wind and w measurement, nor the measurement error of w. Since the variance of w is generally much smaller than that of the horizontal wind, while its measurement error is comparable to that of the radial wind, assuming $w = 0$ is a better way to calculate horizontal winds and that is the method we used in this study. For example, the zonal wind u can be determined when the beam was pointed in the eastward off-zenith direction as

$$u = V_E / \sin\theta.$$

The error in the zonal wind was calculated according to the equation

$$\Delta u = \{\Delta V^2 + w_{rms}^2 \cos^2\theta\}^{1/2} / \sin\theta.$$

It consists the radial wind measurement error ΔV and the error introduced by the assumption of $w = 0$, which is w_{rms}, the root mean square (rms) of w. Similar equations apply to other directions.

2.3. Data preparation

As discussed above, the meteor radar wind is obtained at 6 km vertical resolution and 1 h temporal resolution and is an average over almost the entire sky. The lidar wind has higher vertical (500 m) and temporal (6 min) resolutions. It measures wind only at a small volume of atmosphere (100 m diameter) and about 15 km away from zenith. In this study, the meteor radar winds were determined in two height ranges of 82–88.5 km and 88.5–96 km. The effective mean height of each layer are not at the midpoint because the meteors have a peak in count rate at around 89–90 km, so that the weightings in these two altitude regions produce an effective height for our wind determinations at around 86 and 93 km, respectively. To match the meteor radar wind, the lidar winds were averaged between 84–88 km and 90–96 km and binned to the same 1-h window as the meteor radar wind. The average uncertainty of this averaged lidar wind is about 1.1 and 0.6 ms^{-1} for the 86 and 93 km regions, respectively.

The meteor radar ran continuously throughout the years, except for short periods of power failures and other system downtimes. The Na lidar was operated during the new moon period for several nights in each month. Table 1 lists the dates and times when both lidar and meteor radar winds are available. There are 20 nights when there was at least one temporally and spatially coincident data point. Except for the

Table 1
Number of coincident samples available in each night at 86 and 93 km altitude

Date	86 km	93 km
Sep 22/98	1	2
Sep 24/98	2	2
Sep 26/98	1	1
Jan 12/99	6	4
Jan 14/99	10	7
Jan 15/99	10	8
Feb 20/99	5	3
Apr 16/99	4	2
Apr 17/99	6	5
Apr 18/99	9	5
May 12/99	9	7
May 13/99	9	6
May 14/99	9	7
Nov 11/99	7	6
Nov 12/99	7	8
Nov 15/99	0	6
Dec 06/99	6	3
Dec 07/99	11	6
Jan 05/00	8	4
Jan 06/00	9	5
Total	129	97

3 nights in September 1998, there are at least three coincident data points at one altitude region in each night. Fig. 1 shows the distribution of data points throughout each hour and calendar month. The data points at 86 km is relatively evenly distributed while the 93 km has more data in the later part of the night. There are little data in summer and fall. Most data are in winter months.

3. Comparison methods

Our main objective here is to determine whether the lidar and meteor radar wind measurements are consistent with each other and how much they differ. We compare three aspects of the two measurements. First is their mean values. The mean values are examined with Student T-test to determine if they are significantly different. Second is their correlation. This compares the variability of wind fields measured by the two instruments. The variability comes from intrinsic instrument errors as well as natural atmospheric variability. Because the two instruments are measuring different volumes of the atmosphere, their measurements have inherit differences in addition to instrument errors. We extend the traditional correlation and regression technique to take this into account. This technique is discussed in detail below. The last aspect we compare is the measured tidal variation. The tidal variation is the dominant variability in mesopause region in midlatitude. By averaging data at every hour from all nights, we exclude fluctuations that are quasi-random, such as from gravity waves, and create a "composite" measurement over the night. This "composite" wind measurements are compared to see how well the tidal variation is captured by both instruments.

3.1. Correlation and regression analysis

Regression and correlation methods are commonly used to compare two data sets. Because errors exist in both data sets, it is not appropriate to calculate the regression by simply using one data set as dependent variable and the other as independent variable. A variety of methods exist in the literature to deal with such situations (e.g. York, 1966; MacDonald and Thompson, 1992; Babu and Feigelsen,

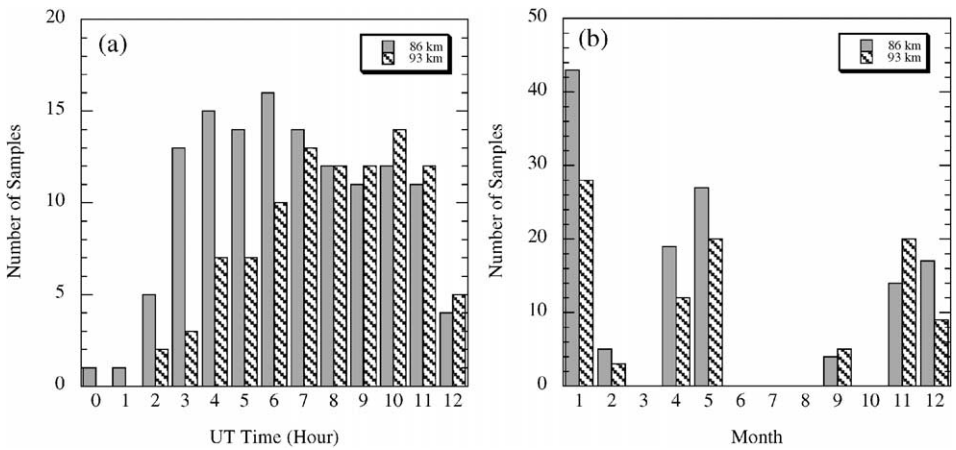

Fig. 1. Number of coincident samples in each hour (a) and in each month (b) at 86 and 93 km altitude. Hours in the plot indicate the beginning of each 1 h window.

1992; Feigelsen and Babu, 1992), but each uses slightly different approximations. In our case, we cannot assume that we know the errors of each technique absolutely, because additional differences arise due to spatial differences between the two instruments. A somewhat broader scope was needed for our studies. Therefore we used a new technique which will form the basis of our correlation studies. The technique described below is based on Thayaparan and Hocking (1998) and Hocking et al. (2001b). We also note at this point that the discussion corrects some erroneous extrapolations made in Thayaparan and Hocking (1998). (That work is valid up to and including their Eq. (9), but attempts to achieve too much beyond that point.) This technique provides a more generalize model that can describe the relations among the measurement and their corresponding errors.

We denote the two data sets as $\{x_i\}$ and $\{y_i\}$ for $i=1\ldots N$. The two data sets are from two instruments that measure the same physical quantity but have different sensitivities to its variabilities. The variability that both instruments can detect is denoted by v_i and $g_0 v_i$ for the two instruments, respectively, where g_0 is a constant, unknown gain. The model equations are

$$x_i = v_i + \delta x_i, \tag{6}$$

$$y_i = g_0 v_i + \delta y_i, \tag{7}$$

where δx_i and δy_i are deviations. g_0 is a measure of the relative amplitude of the variability in two measurements. In essence, we have separated the measurements into two parts, the fully correlated parts (first terms on the right-hand side (RHS)) and uncorrelated parts (second terms on the RHS). The fully correlated parts are the physical variability detectable by both instruments. The uncorrelated parts, δx_i and δy_i, come from the instrumental errors and part of the physical variabilities that detectable by only one instrument but not the other. As discussed in Section 2, the lidar and meteor radar are measuring different volumes of the atmosphere. It is expected that their measurements would respond differently to the natural variabilities of atmosphere because their different spatial averaging. Based on this model, we can derive from measurement the relations among g_0, and variances of v_i, δx_i and δy_i.

We assume $\{\delta x_i\}$ and $\{\delta y_i\}$ are zero mean random variables with normal distribution, and $\{v_i\}$, $\{\delta x_i\}$ and $\{\delta y_i\}$ are mutually independent. By taking square of Eqs. (6) and(7), and multiplying Eqs. (6) and (7), we get

$$s_x^2 = \Sigma_v^2 + \sigma_x^2, \tag{8}$$

$$s_y^2 = g_0^2 \Sigma_v^2 + \sigma_y^2, \tag{9}$$

$$s_{xy}^2 = g_0 \Sigma_v^2, \tag{10}$$

where s_x^2, s_y^2, Σ_v^2, σ_x^2 and σ_y^2 are variances of $\{x_i\}$, $\{y_i\}$, $\{v_i\}$, $\{\delta x_i\}$ and $\{\delta y_i\}$, respectively, and s_{xy}^2 is the covariance between $\{x_i\}$ and $\{y_i\}$. Here we have replaced the ensemble-averaged quantities with sample expectations.

s_x^2, s_y^2, and s_{xy}^2 can be calculated from data samples, so Eqs. (8)–(10) have four unknowns, $\Sigma_v^2, \sigma_x^2, \sigma_y^2$, and g_0. If $\{x_i\}$ and $\{y_i\}$ are measurements of a same physical parameter, then $g_0 = 1$ and Σ_v^2, σ_x^2 and σ_y^2 can be uniquely determined. If that is not the case, as in our study here, then functional relations among $g_0, \Sigma_v^2, \sigma_x^2$ and σ_y^2 can be derived.

In many studies of regression, it is common to treat one variable as if it has no error, and assume all the error is associated with the second variable. This is equivalent to setting either $\sigma_x = 0$ or $\sigma_y = 0$ in Eq. (8) or (9). For $\sigma_x = 0$, we can get

$$g_0(\sigma_x = 0) = s_{xy}^2/s_x^2 = g_x, \tag{11}$$

and for $\sigma_y = 0$,

$$g_0(\sigma_y = 0) = s_y^2/s_{xy}^2 = g_y. \tag{12}$$

Here g_x and $1/g_y$ are slopes of the standard least-square fit line. It is easy to derive that g_x and g_y are related to the correlation coefficient R as

$$R^2 = \left(\frac{s_{xy}^2}{s_x s_y}\right)^2 = g_x/g_y. \tag{13}$$

When neither σ_x nor σ_y can be assumed to be zero, as in our case here, one can only get functional relations between g_0 and σ_x and σ_y as:

$$\sigma_x^2 = s_x^2 - s_{xy}^2/g_0 = s_x^2(1 - g_x/g_0), \tag{14}$$

$$\sigma_y^2 = s_y^2 - s_{xy}^2\ g_0 = s_y^2(1 - g_0/g_y). \tag{15}$$

When $\{x_i\}$ and $\{y_i\}$ are perfectly correlated, $R = 1$ and $g_x = g_y = g_0$. When $0 < R < 1$, we have $g_x < g_0 < g_y$. Therefore g_x and g_y are lower and upper bounds of g_0, respectively. The lower (upper) bound is reached when $\sigma_x = 0$ ($\sigma_y = 0$).

We need to address the meaning of σ_x and σ_y. If we are using two instruments to measure the same quantity, then these two variables tell us the measurement error in each instrument. However, in many situations we cannot measure exactly the same quantity with two different instruments. The comparison between the lidar and meteor radar wind measurements here is one such example. The lidar measures in a volume of atmosphere that is about one hundred meters across, while the radar measures over a region of perhaps a 100 km or more. Thus σ_x and σ_y not only reflect the intrinsic measurement errors of each instrument, but also contain information about the difference between the actual quantities that two instruments are measuring. This difference however, depends on the value of g_0. Changing the value of g_0 gives different values of σ_x and σ_y for different assumptions. For example, by setting $g_0 = 1$, we assume that the fully correlated part has the same amplitude of variability; By setting $g_0 = g_x$, we assume that σ_x contains only the measurement error and σ_y contains both the error of the second instrument and the difference of the two quantities

measured by the two instruments. Another special case is when $\sigma_x = \sigma_y, g_0$ becomes

$$g_0 = \tfrac{1}{2}(g_y - 1/g_x) + \sqrt{1 + \tfrac{1}{4}(g_y - 1/g_x)^2}. \quad (16)$$

This is the same as the slope obtained with total regression, which seeks to minimize the sum of the squared distance from the data point perpendicular to the regression line. The general relations determined by Eqs. (14) and (15) include all the special cases above.

4. Results

We first compare the mean values of the wind between lidar and meteor radar measurement at 86 and 93 km region for both the zonal and meridional components to see if they are consistent. The mean values, their standard deviations and p values of Student T-test are listed in Table 2. The p value is the probability of observing the given samples if their mean values are the same. Since all the p values are significantly larger than 5% (a commonly used threshold), we cannot reject the hypothesis that the mean values of the lidar and meteor radar wind are the same. The mean values at 86 km appear to have better agreement (closer means and larger p) than that at 93 km. This is probably due to stronger wave activities at higher altitude, which could increase the errors in the means.

Next we apply the algorithm described in previous section to the wind data to examine their correlation. Fig. 2 are scatter plots and least-square fit lines for all data samples. The correlation coefficients are also shown. Since we choose to plot lidar wind as the x-axis and meteor radar wind as the y-axis, all the variables with subscript $x(y)$ in previous section correspond to lidar (meteor radar) winds. The slopes of the two lines in each plot in Fig. 2 are $g_x = g_{\text{lidar}}$ and $g_y = g_{\text{radar}}$, respectively, with g_{radar} always larger than g_{lidar} (because of our choice of abscissae). The correlation coefficients vary between 0.63 and 0.70. These values indicate that the two instruments are making consistent measurements, considering that the lidar measures only a small part of the atmosphere, while the radar measures the entire sky, and there are substantial atmospheric perturbations that create spatial variations of the wind field.

Fig. 3 shows the functional relations described by Eqs. (14) and (15). They show the relationship between the three variables $g_0, \sigma_{\text{lidar}}$ and σ_{radar}. The intersects of the curves with the y-axis are g_{lidar} and g_{radar}, with g_{radar} always larger than g_{lidar}. They are the limits of allowable values for g_0. Table 3 lists the values of g_{lidar} and g_{radar}, as well as $g_0, \sigma_{\text{lidar}}$ and σ_{radar} for the special cases of $g_0 = 1$ and $\sigma_{\text{lidar}} = \sigma_{\text{radar}}$. It should be again emphasized that the standard deviations (errors) shown in the scatter plots are not just estimated errors of the measurement, but contain extra effects. They are the standard deviations that are required for the two data sets to have the corresponding g_0 determined by the curve. Although we cannot say exactly which point on the curve best represents our data, these curves do place reasonable limits on allowable values of g_0. If we assume that the lidar and the meteor radar have the same response to the wind variability *they both can measure*, then $g_0 = 1$, and Table 3 tells us that in this case, for u at 86 km, $\sigma_{\text{lidar}} = 18\ \text{ms}^{-1}$ and $\sigma_{\text{radar}} = 12\ \text{ms}^{-1}$. These are the standard deviations which include the measurement errors and variabilities in the atmosphere that cannot be measured by both instruments. Alternatively, we can assume that the intrinsic instrumental errors are small, so $\sigma_{\text{radar}} \approx \sigma_{\text{lidar}}$, because they are mostly from the same spatial variability. Then we have another set of solutions, e.g. for u at 86 km, $\sigma_{\text{lidar}} = \sigma_{\text{radar}} = 15\ \text{ms}^{-1}$ and $g_0 = 0.82$. This solution tells us that under this assumption, the variability of the meteor radar wind is generally smaller than that of the lidar winds (because $g_0 < 1$). A key point to note is that in all cases "$g_0 = 1$" lies within the possible extreme values defined by g_{lidar} and g_{radar}. Therefore we cannot reject the hypothesis that $g_0 = 1$, and the instruments are making consistent measurement of the same wind field.

Note in Table 3 and Fig. 3 that for "$g_0 = 1$", σ_{lidar} are larger than σ_{radar} in 3 of the 4 comparisons, namely for the cases of the meridional wind at 93 km, and the zonal and meridional winds at 86 km. Equivalently, g_0 is < 1 when $\sigma_{\text{radar}} = \sigma_{\text{lidar}}$ in these 3 comparisons. This is consistent with the fact that the lidar measures in a smaller volume of the atmosphere, and therefore lidar winds are more susceptible to atmospheric perturbations. The meteor radar winds are average over the entire sky, therefore tend to have smaller variability. The zonal wind at 93 km, however, is the opposite of the other three. The reason for this is not clear.

Table 2
Mean and standard deviations (s) of wind measurements and their p values from Student T-test

	Na lidar (ms^{-1})		Meteor radar (ms^{-1})		p value
	mean	s_{lidar}	mean	s_{radar}	
u (86 km)	7.3 ± 2.4	27.5	8.9 ± 2.1	24.1	0.64
v (86 km)	-1.1 ± 2.4	27.6	2.0 ± 1.9	21.4	0.32
u (93 km)	18.0 ± 3.3	32.1	12.2 ± 3.6	35.4	0.23
v (93 km)	11.3 ± 2.8	27.7	6.5 ± 2.4	24.0	0.20

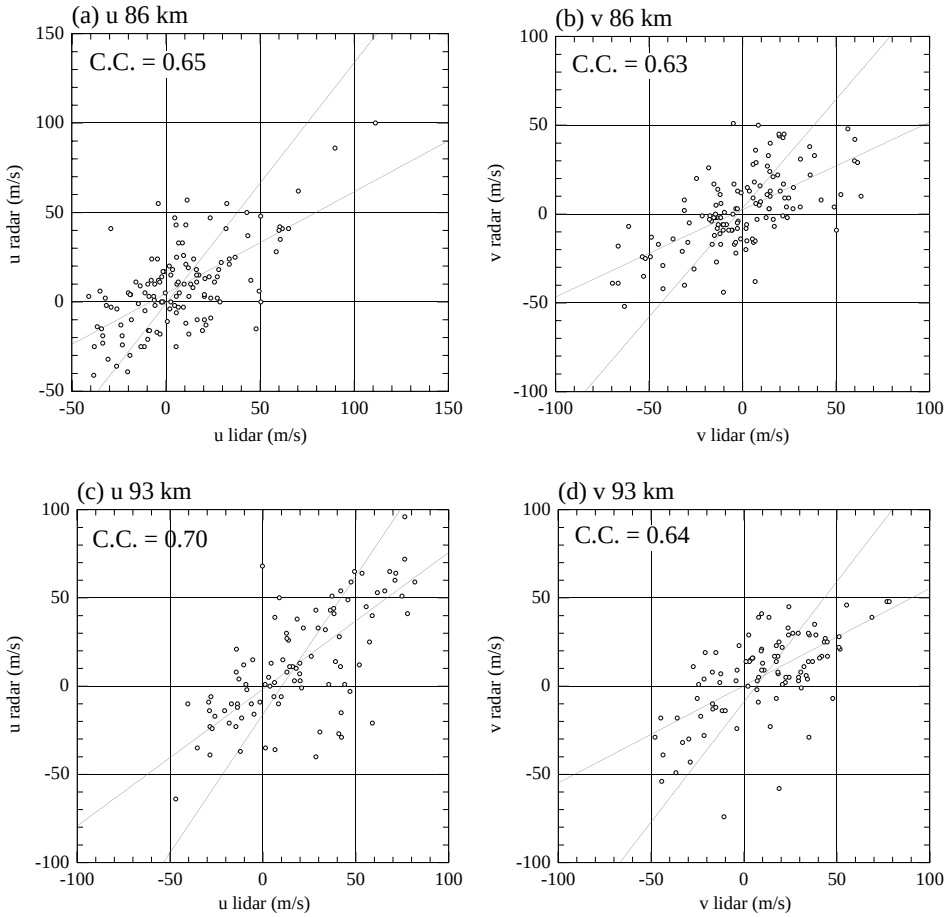

Fig. 2. Scatter plots and least-square line fit for the zonal and meridional wind at 86 and 93 km region. Correlation coefficients are also shown.

Given its large correlation coefficient, it could be that the mean or large scale u are dominant in this altitude region so that other perturbations are relatively small. In this case the instrumental errors might be more important, and the larger instrumental uncertainties of the meteor radar winds could contribute a greater effect to σ_{radar}. The unusually large standard deviation for u at 93 km from meteor radar wind (Table 2) also suggests that.

Finally, we compare the averaged wind variation over the night. The mesospheric wind is strongly influenced by tidal waves, which have horizontal wavelengths much larger than the scale of the atmospheric volume observed by both the meteor radar and the Na lidar. Therefore the tidal variabilities should be easily detected by both instruments. By averaging measurement at every hour from all available nights, we get a "composite" wind over the night. Some early night (before 0300 UT) data has only one or two data samples and therefore are not included (see Fig. 1a). We compare these averaged wind to see if the tidal variabilities are captures consistently by both instruments. These averaged wind are shown in Fig. 4. It can be seen that there are strong tidal variations over the night in all four wind components. Measurements from both instruments are very close to each other. Both instruments give very similar phase and amplitude measurement of the tides. The correlation coefficients range from 0.84 to 0.95, confirming the very high correlations. This indicates that on average, both instruments give similar (and therefore likely reliable) measurement of this dominant atmospheric variability. It is also noted that the difference between lidar and meteor radar winds at any instant can still be very large. The average rms of lidar and meteor radar wind difference is about 20 ms^{-1}. This is mainly due to strong gravity wave activities, which can be easily detected by lidar but are not as sensitive to the meteor radar.

5. Conclusions

We have compared 20 nights of hourly wind measurements made simultaneously by Na lidar and meteor radar at

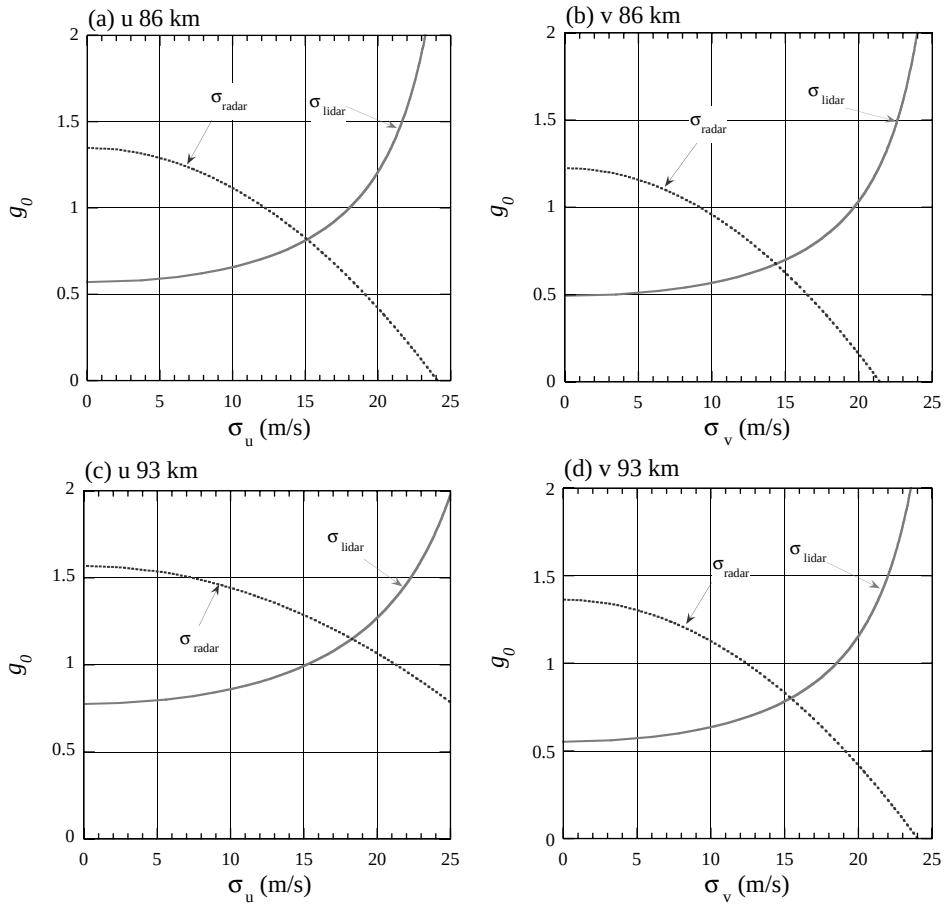

Fig. 3. Relations between g_0 and the errors σ for u and v at 86 and 93 km.

Table 3
Regression parameters in Fig. 3

	$\sigma_{\text{lidar}} = \sigma_{\text{radar}}$		$g_0 = 1$		g_{lidar}	g_{radar}
	g_0	σ	σ_{lidar}	σ_{radar}		
u (86 km)	0.816	15.14	18.06	12.25	0.569	1.348
v (86 km)	0.675	14.37	19.69	9.18	0.492	1.225
u (93 km)	1.149	18.29	15.20	21.29	0.775	1.568
v (93 km)	0.801	15.43	18.54	12.40	0.552	1.363

SOR. The mean winds have no statistically significant difference based on Student T-test. The correlation coefficients vary between 0.63 and 0.70. Considering the fact that each instrument is measuring different spatial averages, in a wind field which is highly variable both spatially and temporally, we consider these correlation coefficients to be satisfactory. Furthermore, we have applied a novel correlation method to explore the relationship between the lidar and meteor radar winds. We have shown that the instruments are making consistent measurements of the same wind field. Errors have been deduced for each instrument, but we emphasize that these errors contain not only instrumental effects, but also contain the effects of the large spatial variability of the wind field. Furthermore, the lidar winds often have larger associated standard deviations because they have higher sensitivity to small-scale perturbations in the wind field. We also compared the wind variation over the "composite" night, which is obtained by averaging wind from all nights at the

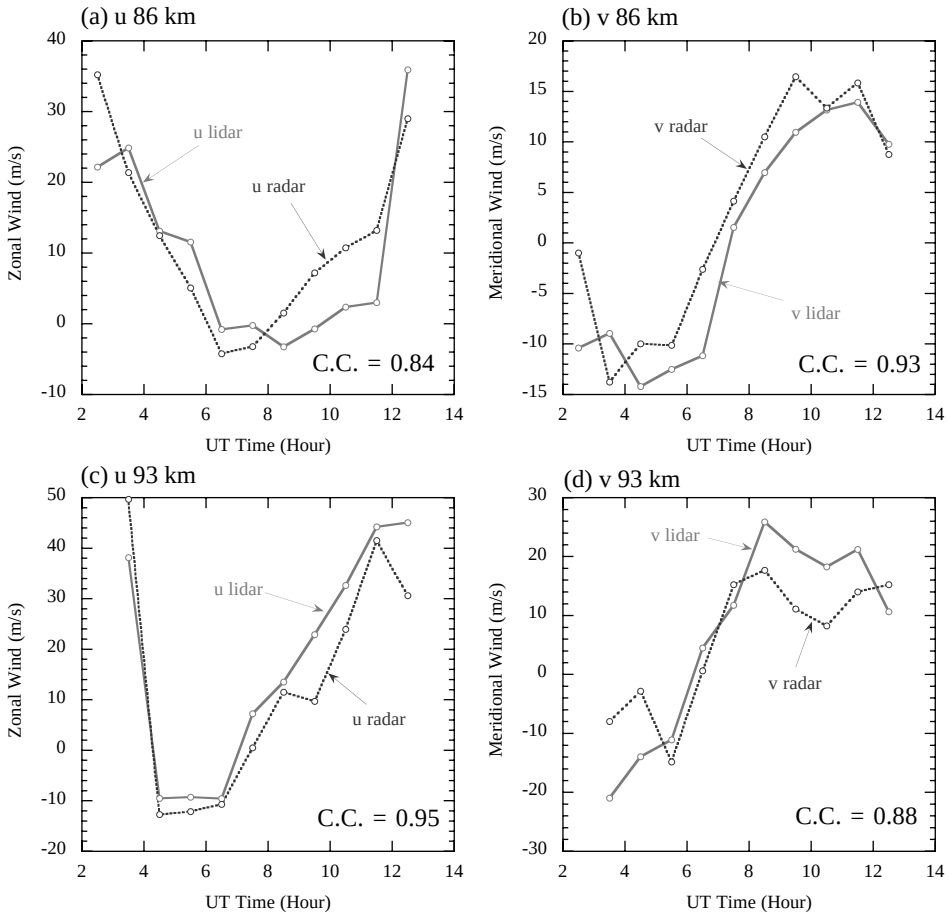

Fig. 4. Comparison of lidar (solid lines) and radar (dotted lines) wind measurements for (a) u at 86 km, (b) v at 86 km, (c) u at 93 km and (d) v at 93 km averaged at every hour. The correlation coefficients are also shown.

same hour. The results show that both instrument can detect the strong tidal variation and give consistent results. Their variations is highly correlated with correlation coefficients range from 0.84 to 0.95. However, the difference between individual hourly measurement can be significant, mainly due to large (small) sensitivity of the lidar (meteor radar) to the strong gravity waves in the mesopause region.

The study provides a guide of the reliability of lidar and meteor radar wind measurements in the mesopause region. Each instrument has its own advantages and disadvantages. Radar measurement can cover both day and night, and run in unattended mode, while lidar measurements can provide detailed vertical and temporal resolution. On averaged, both lidar and radar give very similar measurements. Their mean values and tidal features are consistent and highly correlated. However, there are significant differences when comparing measurements at each individual hour, primarily because the two instruments are measuring different volumes of the atmosphere and therefore have different sensitivity to gravity wave perturbations.

Acknowledgements

Important discussions with Patricia Franke are gratefully acknowledged. The assistance of the staff at Starfire Optical Range, Kirtland Airforce Base, New Mexico, in supporting the instruments used in these investigations is greatly appreciated. The SKiYMET radar used in these studies is fully owned and operated by Mardoc Inc. of Canada, and is leased to the University of Western Ontario. WKH would like to especially thank Owen Mitchell for his support of the radar. Valuable comments by Chester S. Gardner, Xinzhao Chu and Gary Swenson are appreciated. This study is supported in part by NSF Grant ATM-97-09921.

References

Babu, G.J., Feigelsen, E.D., 1992. Analytical and Monte Carlo comparisons of six different linear least-squares fits. Communications in Statistics. Communications in Statistics—Simulation and Computation 21, 533–549.

Bills, R.E., Gardner, C.S., Franke, S.J., 1991a. Na Doppler/temperature lidar: initial mesopause region observations and comparison with the Urbana MF radar. Journal of Geophysical Research 96, 22,701–22,707.

Bills, R.E., Gardner, C.S., She, C.Y., 1991b. Narrow band lidar technique for sodium temperature and Doppler wind observations of the upper atmosphere. Optical Engineering 30, 13–21.

Briggs, B.H., 1984. The analysis of spaced sensor records by correlation techniques. In: R.A. Vincent (Ed.), Handbook for MAP, Ground Based Techniques, vol. 13, University of Illinois at Urbana-Champaign, Urbana, Illinois, pp. 166–186.

Cervera, M.A., Reid, I.M., 1995. Comparison of simultaneous wind measurements using colocated VHF meteor radar and MF spaced antenna radar systems. Radio Science 30, 1245–1261.

Feigelsen, E.D., Babu, G.J., 1992. Linear regression in astronomy. II. Astro-physical Journal 397, 55–67.

Gardner, C.S., Papen, G.C., 1995. Mesospheric Na wind/temperature lidar. The Review of Laser Engineering 23, 131–134.

Gardner, C.S., Senft, D.C., Beatty, T.J., Bills, R.E., Hostetler, C., 1989. Rayleigh and sodium lidar techniques for measuring middle atmosphere density, temperature and wind perturbations and their spectra. In: Liu, C.H. (Ed.), World Ionosphere/Thermosphere Study (WITS) Handbook. Scientific Committee on Solar Terrestrial Physics, Urbana, Illinois.

Hocking, W.K., Thayaparan, T., 1997. Simultaneous and co-located observation of winds and tides by MF and meteor radars over London, Canada, (43°N, 81°W) during 1994–1996. Radio Science 32, 833–865.

Hocking, W.K., May, P., Roettger, J., 1989. Interpretation, reliability and accuracies of parameters deduced by the spaced antenna method in middle atmosphere applications. Pure and Applied Geophysics 130, 571–604.

Hocking, W.K., Fuller, B., Vandepeer, B., 2001a. Real-time determination of meteor-related parameters utilizing modern digital technology. Journal of Atmospheric and Solar-Terrestrial Physics 63, 155–169.

Hocking, W.K., Thayaparan, T., Franke, S.J., 2001b. Method for statistical comparison of geophysical data obtained by multiple instruments. Advances in Space Research 27, 1089–1098.

Holdsworth, D.A., 1999. Spatial correlation analysis revisited: Theory and application using a radar backscatter model data. Radio Science 34, 629–642.

Jones, J., Webster, A.R., Hocking, W.K., 1998. An improved interferometer design for use with meteor radars. Radio Science 33, 55–65.

MacDonald, J.R., Thompson, J., 1992. Least-squares fitting when both variables contain errors: pitfalls and possibilities. American Journal of Physics 60, 66–73.

Papen, G.C., Pfenninger, W.M., Simonich, D.M., 1995. Sensitivity analysis of sodium narrowband wind-temperature lidar systems. Applied Optics 34, 480–498.

Phillips, A., Manson, A.H., Meek, C.E., Llewellyn, E.J., 1994. A long-term comparison of middle atmosphere winds measured at Saskatoon (52°N, 107°W) by a medium-frequency radar and a Fabry-Perot interferometer. Journal of Geophysical Research 99, 12,923–12,935.

Roper, R.G., 1975. The measurement of meteor winds over Atlanta (34°N, 84°W). Radio Science 10, 363–369.

She, C.Y., Yu, J.R., 1994. Simultaneous three-frequncy Na lidar measurements of radial wind and temperature in the mesopause region. Geophysical Research Letters 21, 1771–1774.

Thayaparan, T., Hocking, W.K., 1998. A least-squares straight-line fitting algorithm with automatic error determination. Technical Note 98-004, Defense Research Establishment, Ottawa, Canada.

York, D., 1966. Least-squares fitting of a straight line. Canadian Journal of Physics 44, 1079–1086.